


COMMUNICATION

Large transient capacitive currents in wild-type lysosomal Cl^-/H^+ antiporter CLC-7 and residual transport activity in the proton glutamate mutant E312A

Michael Pusch and Giovanni Zifarelli 

CLC-7 is a lysosomal $2 \text{Cl}^-/1 \text{H}^+$ antiporter of the CLC protein family, which comprises Cl^- channels and other Cl^-/H^+ antiporters. Mutations in CLC-7 and its associated β subunit Ostm1 lead to osteopetrosis and lysosomal storage disease in humans and mice. Previous studies on other mammalian CLC transporters showed that mutations of a conserved, intracellularly located glutamate residue, the so-called proton glutamate, abolish steady-state transport activity but increase transient capacitive currents associated with partial reactions of the transport cycle. In contrast, we observed large, transient capacitive currents for the wild-type CLC-7, which depend on external pH and internal, but not external, Cl^- . Very similar transient currents were observed for the E312A mutant of the proton glutamate. Interestingly, and unlike in other mammalian CLC transporters investigated so far, the E312A mutation strongly reduces, but does not abolish, stationary transport currents, potentially explaining the intermediate phenotype observed in the E312A mouse line.

Introduction

Human CLC proteins are composed of both Cl^- channels (CLC-1, CLC-2, CLC-Ka, and CLC-Kb) and strictly coupled $2 \text{Cl}^-/1 \text{H}^+$ antiporters (CLC-3–7; Zifarelli and Pusch, 2007; Jentsch and Pusch, 2018). In addition to transporting ions by very different thermodynamic mechanisms, these two subclasses have different subcellular localization, with all CLC channels being expressed at the plasma membrane and the antiporters being expressed mostly in intracellular compartments (Zifarelli and Pusch, 2007; Jentsch and Pusch, 2018; Hryciw et al., 2003). Surprisingly, CLC channels and transporters show a very similar structural architecture: they are formed by dimers with each subunit harboring an independent ion permeation pathway (Fig. 1 A; Dutzler et al., 2002; Dutzler et al., 2003; Park et al., 2017; Park and MacKinnon, 2018; Feng et al., 2010; Wang et al., 2019; Schrecker et al., 2020; Zhang et al., 2020). Residues with a critical role in the transport mechanism are highly conserved among channels and transporters. Different crystal structures have captured the side chain of a conserved glutamate residue—also named gating glutamate, E245 in CLC-7—occupying either the external or the central anion binding sites—in competition with Cl^- ions—or directed away from the permeation pathway toward the extracellular side (Dutzler et al., 2002; Dutzler et al., 2003;

Feng et al., 2010; Schrecker et al., 2020). These movements are voltage, chloride, and proton dependent and underlie the opening and closing of the permeation pathway and the mechanism of proton transport in CLC antiporters (Zifarelli and Pusch, 2007; Jentsch and Pusch, 2018). Substitutions of the gating glutamate with neutral residues abolish gating and proton transport and transform CLC antiporters in purely ohmic chloride conductances (Accardi et al., 2004; Picollo and Pusch, 2005; Scheel et al., 2005; Neagoe et al., 2010; Leisle et al., 2011).

At the intracellular side, another glutamate residue that is highly conserved in human and many prokaryotic CLC transporters (E312 in CLC-7) was originally thought to be essential for proton transport, and therefore also named proton glutamate, and serves as a relay station for proton movement from the intracellular space to the central binding site (Fig. 1 A; Zifarelli and Pusch, 2007; Jentsch and Pusch, 2018). This was supported by the observation that the corresponding residue is a valine in all CLC channels and by the finding that substitution of the proton glutamate with glutamine abolished proton transport in the bacterial CLC-ec1 (Accardi et al., 2005). Substitution of the proton glutamate with alanine ablates overall transport in several CLC transporters (Zdebik et al., 2008; Neagoe et al., 2010),

Istituto di Biofisica, Consiglio Nazionale delle Ricerche, Genoa, Italy.

Correspondence to Giovanni Zifarelli: giovanni.zifarelli@ibf.cnr.it.

© 2020 Pusch and Zifarelli. This article is distributed under the terms of an Attribution–Noncommercial–Share Alike–No Mirror Sites license for the first six months after the publication date (see <http://www.rupress.org/terms/>). After six months it is available under a Creative Commons License (Attribution–Noncommercial–Share Alike 4.0 International license, as described at <https://creativecommons.org/licenses/by-nc-sa/4.0/>).

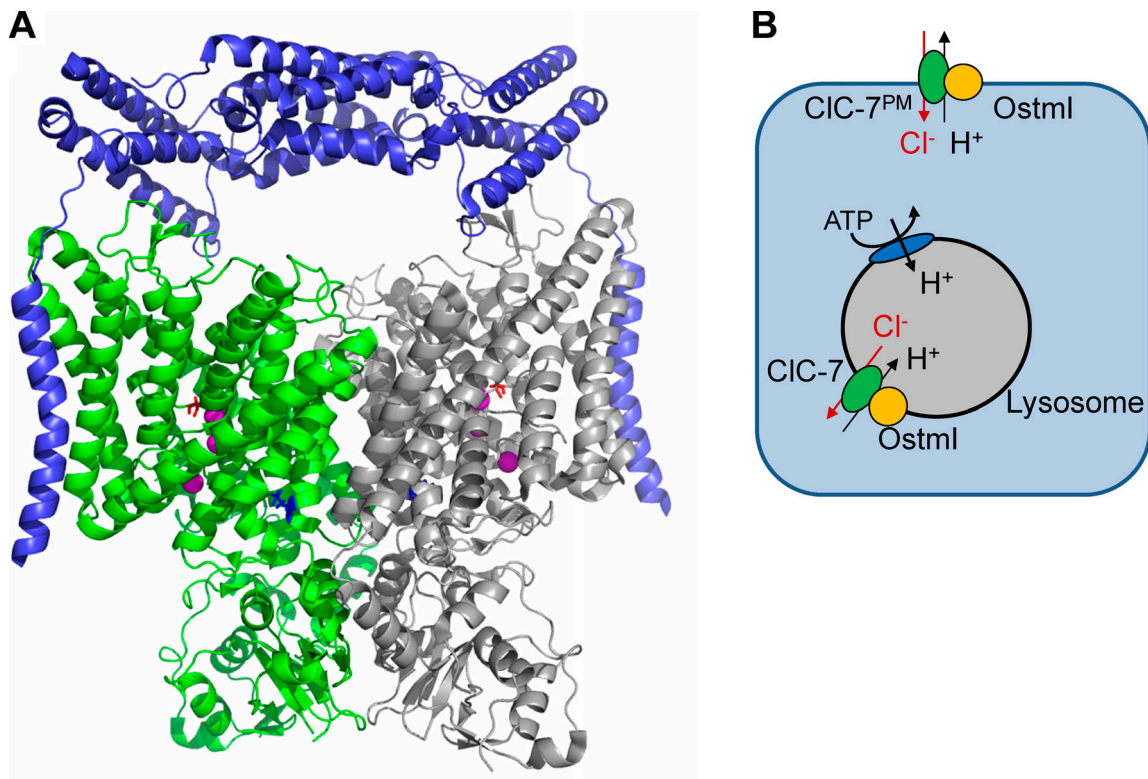


Figure 1. Structure and function of the CLC-7/Ostm1 complex. (A) Dimeric architecture of the CLC-7/Ostm1 complex (Protein Data Bank accession no. 7JM7) viewed from the membrane plane (extracellular side above and cytoplasmic side below). The two subunits of Ostm1 are shown in blue, whereas the two subunits of CLC-7 are shown in green and gray. The proton glutamate, E312 in CLC-7, is shown in blue, the gating glutamate, E245, is shown in red. Anions bound at S_{cen} and S_{int} are represented as magenta spheres. (B) Cartoon illustrating the physiological role of CLC-7 in lysosomes. The coupled Cl^-/H^+ exchange mediated by CLC-7, together with the action of other proteins, establish the acidic lysosomal pH. The present study measures currents resulting from CLC-7 redirected to the plasma membrane by mutation of di-leucine lysosomal targeting motifs. If CLC-7 retains the same topology and voltage dependence in lysosomes and at the plasma membrane, then lysosomal CLC-7 directs Cl^- toward the cytosol. Proof of this concept awaits direct measurements of transport currents in lysosomes.

but it has also been found that substitutions with other non-protonatable residues preserved some coupled Cl^-/H^+ transport (Zdebik et al., 2008; Grieschat and Alekov, 2012; Guzman et al., 2013; Feng et al., 2010). However, the mechanism of proton transport remains much less understood compared with that of Cl^- transport.

Interestingly, although unable to perform steady-state ion transport, the mutant of the proton glutamate in CLC-5, E268A, was able to elicit transient capacitive currents (Smith and Lippiat, 2010), probably due to partial reactions of the transport cycle (Zifarelli et al., 2012; Smith and Lippiat, 2010). These capacitive currents have also been found in CLC-3 and less prominently in CLC-4, and they are also greatly potentiated by substitutions of the proton glutamate (Grieschat and Alekov, 2012; Guzman et al., 2013).

CLC-7 is unique among CLC antiporters in that it is associated in an obligate manner with an accessory β subunit, called Ostm1, a highly glycosylated single-transmembrane domain protein (Lange et al., 2006). The complex formed by CLC-7 and Ostm1 is localized in late endosomal/lysosomal compartments of several tissues and in the ruffled border of bone-resorbing osteoclasts (Fig. 1 B; Lange et al., 2006). Recently, two electron cryomicroscopy studies have elucidated the structure of the complex

formed by CLC-7 and Ostm1 (Schrecker et al., 2020; Zhang et al., 2020). A dimer of glycosylated Ostm1 α helices forms a luminal surface that covers the extracellular side of CLC-7 and protects it from degradation, whereas the single-transmembrane helix of each Ostm1 subunit interacts laterally with both the transmembrane and the cytoplasmic domains of CLC-7 (Fig. 1 A; Schrecker et al., 2020; Zhang et al., 2020). Ostm1 does not induce large-scale structural changes in CLC-7, but it has some effect on the ion permeation pathway with rearrangements in the extracellular side of several α helices and a change of occupancy of the external and central Cl^- binding sites (Schrecker et al., 2020). Zhang et al. (2020) found also that the interaction between Ostm1 and the region at the interface between the transmembrane and the two cystathionine- β -synthase domains affects the slow gating that regulates transport.

Mutations in CLC-7 and Ostm1 cause osteopetrosis and lysosomal storage disease associated with retinal and hippocampal degeneration in humans and mice (Lange et al., 2006; Kasper et al., 2005; Kornak et al., 2001). In mice, in an agouti genetic background (yellow fur), CLC-7 loss-of-function mutations also lead to a change of fur color to gray (Lange et al., 2006). The greatly reduced CLC-7 protein level observed in mice lacking functional Ostm1 suggests that Ostm1 is important for CLC-7/

Ostm1 complex stability (Lange et al., 2006), but it has also emerged that CLC-7 determines the targeting of Ostm1 (Lange et al., 2006; Stauber and Jentsch, 2010). It was initially hypothesized that CLC-7 could assist in the acidification of intracellular compartments mediated by V-type ATPases by providing a Cl^- shunting conductance (Kornak et al., 2001); however, the specific molecular function of CLC-7 has been difficult to pin down because the intracellular localization precluded a detailed biophysical investigation. Lysosomal pH was normal in cells lacking either CLC-7 or Ostm1 (Kornak et al., 2001; Kasper et al., 2005). In native lysosomal preparation, Graves et al. (2008) reported that knockdown of CLC-7 by small interfering RNA impaired Cl^- accumulation and strongly reduced acidification in a manner that was consistent with a 2 Cl^- /1 H^+ transport stoichiometry, rather than with a Cl^- shunt conductance. Decisive progress was made with knock-in (KI) mice harboring the gating glutamate mutation E245A that turns CLC-7 into a Cl^- channel (Weinert et al., 2010). These mice had lysosomes with normal pH, but reduced chloride concentration, and their phenotype was similar to that of mice lacking CLC-7 (Weinert et al., 2010). This conclusively showed that the Cl^-/H^+ antiport activity of CLC-7 is essential for lysosomal function (Fig. 1B). To test whether CLC-7 has physiological functions that are not related to its ion transport activity, Weinert et al. (2014) generated a mouse KI line harboring the charge-neutralizing mutation of the CLC-7 proton glutamate (E312A). The underlying assumption was that this mutation abolishes transport activity, as indicated by functional measurements of the mutant in *Xenopus laevis* oocytes (Leisle et al., 2011) and as observed in other CLC transporters (Zdebik et al., 2008; Neagoe et al., 2010). Nevertheless, the mutant preserved CLC-7 protein expression and targeting (Weinert et al., 2014). Interestingly, these KI mice displayed a phenotype that was intermediate between WT mice and CLC-7 knockout (KO) mice with an osteopetrosis similar to KO but with a milder neurodegeneration and with a fur color as that of WT (Weinert et al., 2014). This suggested that CLC-7 could indeed have a physiological role independent of its transport activity, and it was speculated that CLC-7 could serve to assemble macromolecular protein complex on the lysosomal membrane (Weinert et al., 2014).

The biophysical characterization of CLC-7 made tremendous progress after the finding that the lysosomal localization was mostly due to the presence of several N-terminal di-leucine targeting motifs that, when neutralized by alanine mutation (the construct was named CLC-7^{PM}), lead to a partial expression at the plasma membrane (Stauber and Jentsch, 2010). This targeting was sufficient to measure transmembrane currents with standard electrophysiological techniques in oocytes and HEK293 cells. The observed CLC-7^{PM}/Ostm1 currents were strongly outwardly rectifying with a slow gating of ion exchange activity (Leisle et al., 2011).

Here, by using patch-clamp measurements on HEK293 cells, we observe for the first time transient capacitive currents from CLC-7^{PM} and the mutant E312A^{PM}, henceforth simply indicated as CLC-7 and E312A. Surprisingly, and different from the other CLC antiporters characterized so far, the proton glutamate mutation to alanine (E312A) does not abolish transport activity.

These results provide novel insight into the biophysical mechanism of ion transport in CLC-7 and potentially explain the elusive phenotype of the E312A KI mouse line. The identification of transient capacitive currents provides a new tool with which to investigate the molecular basis of the CLC-7 transport mechanism.

Materials and methods

Molecular biology and heterologous expression

Coexpression of CLC-7 and Ostm1 was obtained using the construct described by Zanardi et al. (2013), in which Ostm1 is connected to the CLC-7 DNA by a self-cleaving 2A peptide and cloned in the pFrog vector for expression in HEK293 cells (Günther et al., 1998). A fluorescent protein was fused to the C terminus of CLC-7 to allow for the detection of positively transfected cells. All original clones were kindly provided by T.J. Jentsch (Leibniz-Forschungsinstitut für Molekulare Pharmakologie and Max Delbrück Center for Molecular Medicine, Berlin, Germany). For CLC-7, four mutations were introduced to neutralize lysosomal-targeting di-leucine motifs (leucine at positions 23, 24, 36, and 37). The resulting construct has been shown to cause partial redirection to the plasma membrane (Stauber and Jentsch, 2010) and is henceforth indicated as simply WT CLC-7. The mutations E312A and R760Q were introduced in this background—and will be simply indicated as E312A and R760Q—by recombinant PCR as described previously (Accardi and Pusch, 2003). HEK293 cells were cultured in Dulbecco's modified Eagle's medium with 1% glutamine, 1% penicillin/streptomycin, and 10% FBS (all from Euroclone). Transfection was performed with the Effectene kit (Qiagen), and measurements were performed 24–72 h after transfection.

Electrophysiology

Patch-clamp experiments were performed in the whole-cell configuration. Pipettes were pulled from borosilicate capillaries (Hilgenberg) and had a resistance of 1.5–2.5 MΩ in measuring solutions. The standard intracellular (pipette) solution contained (in mM) 130 NaCl, 10 HEPES, 2 MgSO_4 , and 2 EGTA (pH 7.3). For experiments with low intracellular $[\text{Cl}^-]$, 110 mM of NaCl were substituted with an equimolar amount of Na-glutamate. The extracellular (bath) solution contained (in mM) 147 NaCl, 10 HEPES, 4 Ca-gluconate, 10 HEPES, 2 MgCl_2 , and 1 EGTA (pH 7.3). In the experiments with $[\text{Cl}^-]_{\text{ext}} = 0$, NaCl was substituted by Na-glutamate to lower the Cl^- concentration. In these experiments, a salt bridge (1% agar/3 M KCl) was used to connect the ground electrode to the bath solution. pH was adjusted using NaOH or H_2SO_4 to the desired values. Mes buffer was used for pH 6.3 and bis-tris-propane buffer for pH 8.3 instead of HEPES. Measurements were performed by applying the extracellular solutions through a 0.5-mm-wide plastic tubing positioned close to the cell.

The voltage protocols used to stimulate the cells are reproduced as insets in the figures. Briefly, to measure transient capacitive currents, we used a P/N subtraction procedure (see below) applied to two different voltage protocols. One consisted of voltage steps from 200 mV to −40 mV in decrements of 10

mV. Voltage steps had a 5-ms duration. The other protocol was similar, but the voltage steps were of a 100-ms duration and ranged from 160 mV to −100 mV in 20-mV decrements. To measure the dependence of the transient capacitive currents on the duration of the activating pulse, a voltage pulse to 140 mV was applied with a variable duration ranging from 0.1 to 333 ms.

To measure steady-state transport currents from WT, the protocol consisted of voltage steps of a 1-s duration from 120 to −40 mV in decrements of 20 mV. No leak subtraction was performed for this protocol. Holding potential was 0 mV in all the measurements.

Data were acquired at 100 kHz after filtering at 10 kHz with an eight-pole Bessel filter using an Axopatch 200 amplifier (Molecular Devices). Acquisition was performed at room temperature with the custom program GePulse, and data analysis was performed by using the custom program Ana (both available at the Pusch laboratory webpage), SigmaPlot (Systat Software), and ORIGIN 2015 (OriginLab). Molecular models were represented with the program Pymol (Schrödinger Inc.). If not otherwise stated, error bars indicate SEM. Statistical differences were assessed by using Student's *t* test (*P* < 0.05).

P/N subtraction procedure

To measure transient capacitive currents, a P/N subtraction protocol was applied to measure and subtract capacitive artifacts. The P/N protocol is a scaled version of the voltage protocol (scaling factor = 0.2) applied with an inverted sign. This means that if a voltage protocol consists of steps from 160 mV to −100 mV, the relative P/N protocol goes from 20 mV to −32 mV. The currents obtained with the P/N protocol can be subtracted off-line from the currents obtained with the standard voltage protocol, allowing the subtraction of the capacitive artifacts that would mask the transient capacitive currents (e.g., see Fig. S3).

Statistical analysis

Steady-state charge-voltage relationships—*Q(V)* curves—were constructed by integrating the current responses at a constant tail voltage that followed the activating voltage steps (e.g., see Fig. 2).

The *Q(V)* was fitted with a Boltzmann function (e.g., see Fig. 2) of the form

$$Q(V) = \frac{Q_{\max}}{1 + e^{zF(V_{1/2} - V)/RT}},$$

where *z* is the apparent gating valence of the process, *V*_{1/2} the voltage of half-maximal activation, and *F*, *R*, and *T* represent the Faraday constant, the gas constant, and the absolute temperature, respectively.

Online supplemental material

Fig. S1 shows representative measurements from WT CLC-7. Fig. S2 illustrates the correlation between ionic current and the charge associated with transient capacitive currents for WT and E312A. Fig. S3 shows the effect of the P/N subtraction protocol on currents from nontransfected cells. Fig. S4 shows the effect of the P/N subtraction protocol on currents from E312A and demonstrates that the small currents observed in the negative

voltage range are due to leak. Fig. S5 demonstrates that the E245A mutation abolishes transient capacitive currents.

Results

CLC-7 mediates transient capacitive currents

Upon coexpressing the plasma membrane-targeted CLC-7 and Ostml in HEK293 cells, large, slowly activating outward currents can be observed at positive voltages (Fig. S1; Leisle et al., 2011). Here, using high-time resolution short voltage-clamp protocols, we discovered the additional presence of large, transient capacitive currents (Fig. 2). These transient currents are not visible using the standard long voltage-clamp protocol (Fig. S1; Leisle et al., 2011), but rather require the application of P/N subtraction voltage protocols to subtract leak and linear capacitive current (see Materials and methods). In the presence of extracellular Cl[−], biphasic currents are elicited by steps to positive voltages, whereas upon return to the holding voltage of 0 mV, large transient inward currents are measured. As the holding voltage was close to the reversal potential expected for 2 Cl[−]/1 H⁺ antiport, the transient inward currents cannot reflect net membrane transport but are of capacitive nature. In the absence of Cl[−], upon voltage steps to positive voltages, steady-state currents are abolished, but outward capacitive currents become clearly visible. The inward capacitive currents upon return to the holding voltage are unaffected by the absence of extracellular Cl[−]. Wash with Cl[−]-containing solution restores the initial situation (Fig. 2 A). The limited time resolution of the whole-cell recordings precludes a quantitative analysis of the kinetics of the transient currents. Yet, information on the voltage dependence can be obtained by analyzing the charge-voltage relationship, *Q(V)*, as measured from the integral of the transient inward currents. Performing fits with a Boltzmann function (see Materials and methods), we obtained the values of *V*_{1/2} and *z* of *Q(V)* under different experimental conditions (Fig. 2 B). The procedure is illustrated in Fig. 2 B for a representative cell. Compared with control conditions, the voltage dependence of the charge movement was shifted by ~50 mV toward negative potentials by pH 8.3, whereas pH 6.3 leads to a shift of >40 mV in the opposite direction and it does not allow saturation of the curve in the voltage range we could explore (Fig. 2 B). While the effect at pH 6.3 is qualitatively robust and consistent across our measurements, the lack of saturation makes the quantitative analysis less reliable, and the mean values for *V*_{1/2} and *z* should be considered only indicative in this case (Fig. 2, C and D). Importantly, removal of Cl[−]_{ext} is not associated with a reduction of the amount of charge and has only a small effect on the *Q(V)* (Fig. 2, A and B). Fig. 2, C and D, shows average values of *V*_{1/2} and *z* and further supports these conclusions (*V*_{1/2} values [in mV] are 110.5 ± 7.6 at pH 7.3, 69.1 ± 6.7 at pH 8.3, 148.5 ± 10.1 at pH 6.3, 106.0 ± 3.5 in 0 Cl[−]_{ext}, 59.4 ± 5.6 with 20 mM Cl[−]_{int}, and 78.3 ± 12.9 with 20 mM Cl[−]_{int} at pH 6.3). In contrast to the lack of effect of extracellular Cl[−] on the transient currents, decreasing intracellular Cl[−] from 130 mM to 20 mM causes a 40-mV shift of *V*_{1/2} in the hyperpolarized direction (Fig. 2 C). The effects of extracellular pH_{ext} and Cl[−]_{int} seem to be independent as the shift of *V*_{1/2} induced by acidifying the extracellular pH from 7.3 to 6.3 was similar in

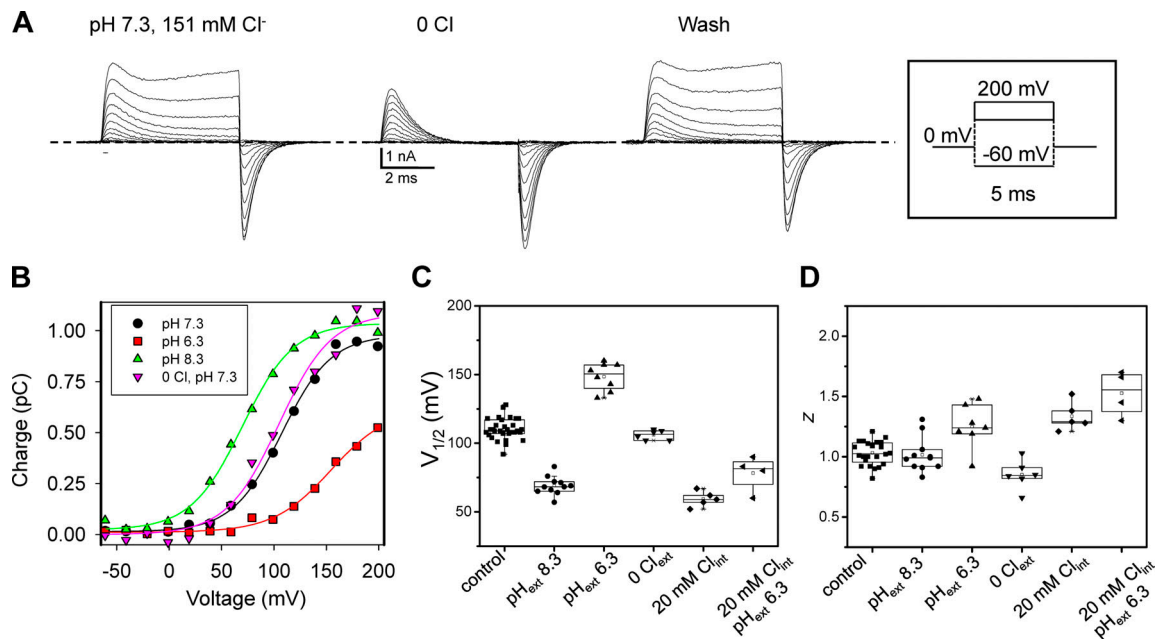


Figure 2. Transient currents of ClC-7. (A) Representative transient currents from ClC-7 in control conditions (left), without extracellular Cl⁻ (middle), and after wash (right). The voltage protocol is shown as inset. Currents were elicited with test pulses of 5-ms duration, and linear leak and capacitive artifacts were subtracted through a P/N voltage protocol (see Materials and methods). (B) Charge measured upon return to the holding voltage (off charge), plotted as a function of the preceding step voltage ($Q(V)$) from the same cell in different extracellular solutions. Lines represent fits with a Boltzmann function (see Materials and methods). (C) Box plots overlaid on original data show mean values of the voltage of half-maximal activation ($V_{1/2}$) derived from the analysis shown in B in different ionic conditions. (D) Box plots overlaid on original data show mean values of the apparent gating charge (z).

130 mM and 20 mM Cl⁻_{int} (Fig. 2 C). The steepness of the Boltzmann distribution has an average value of $z \sim 1.0$ at pH 7.3 and is practically independent of extracellular ionic conditions (Fig. 2 D), suggesting that transient currents are accompanied by the net movement of one elementary charge (Bezannilla, 2008). The relationship between steady-state current and the charge associated with the transient capacitive currents is linear with a slope of $640 \pm 140 \text{ s}^{-1}$ (Fig. S2 A).

Transient capacitive currents in E312A

The finding of large, transient capacitive currents in WT ClC-7 was surprising, and to study them in more detail we mutated the conserved proton glutamate of ClC-7 into alanine (E312A). The corresponding mutation inhibits proton transport in the bacterial ClC-ec1 transporter (Lim and Miller, 2009) and abolishes transport altogether in the mammalian antiporters ClC-3, ClC-4, ClC-5, and ClC-6 (Zdebik et al., 2008; Neagoe et al., 2010; Guzman et al., 2013). In particular, in ClC-5, this mutation (E268A) was used as a tool to isolate and study in detail transient capacitive currents that are almost undetectable in the WT (Smith and Lippiat, 2010; Zifarelli et al., 2012).

Unexpectedly, we found that for ClC-7 the mutation E312A strongly reduces but does not abolish transport activity (see Steady-state currents in E312A). In any case, the mutation exhibits large, transient capacitive currents similar to those of WT ClC-7, shown in Fig. 3, A and B, for two different voltage protocols.

As for ClC-7, removal of Cl⁻_{ext} abolishes steady-state currents, makes the outward capacitive currents clearly visible, and leaves the inward capacitive currents basically unaffected (Fig. 3).

To compare the biophysical properties of the transient currents of E312A with those of the WT, we analyzed the currents elicited by the same voltage protocol (test pulse duration of 5 ms as shown in Fig. 3 A). Fig. 3 C shows the $Q(V)$ relationship for the representative currents in Fig. 3 A and indicates that as for the WT, removal of Cl⁻_{ext} leaves the $Q(V)$ of E312A basically unaffected. This conclusion is confirmed by the statistical analysis of $V_{1/2}$ (Fig. 3 D) and z (Fig. 3 E). The value of $V_{1/2}$ for E312A at pH 7.3 is 108.8 mV and almost identical to WT (110.5 mV; Fig. 2 C).

Fig. 4 illustrates the effects of pH on the transient currents of E312A (the effects on steady-state currents are described in the following paragraph). Consistent with WT, alkaline pH causes a hyperpolarizing shift of the $V_{1/2}$ and acidic pH causes a depolarizing shift (Fig. 4 B), whereas there is no major effect of pH on z (Fig. 4 C). In Fig. 4, B and C, the values at pH 7.3 are shown as dashed lines for comparison.

As discussed below, [Cl⁻]_{ext} and pH_{ext} dependence are somewhat different from that found for the transient capacitive currents of the proton glutamate mutant (E268A) of ClC-5, which were less dependent on pH but more strongly dependent on Cl_{ext} (Zifarelli et al., 2012). To investigate possible differences between the mechanisms generating transient currents in ClC-5 and ClC-7, we mutated the gating glutamate of ClC-7 to alanine (E245A). We found that this mutation turns ClC-7 into a purely ohmic conductance, consistent with Leisle et al. (2011), and did not show any transient capacitive current (Fig. S5). This supports the critical role of the gating glutamate in generating the transient capacitive currents of ClC-7.

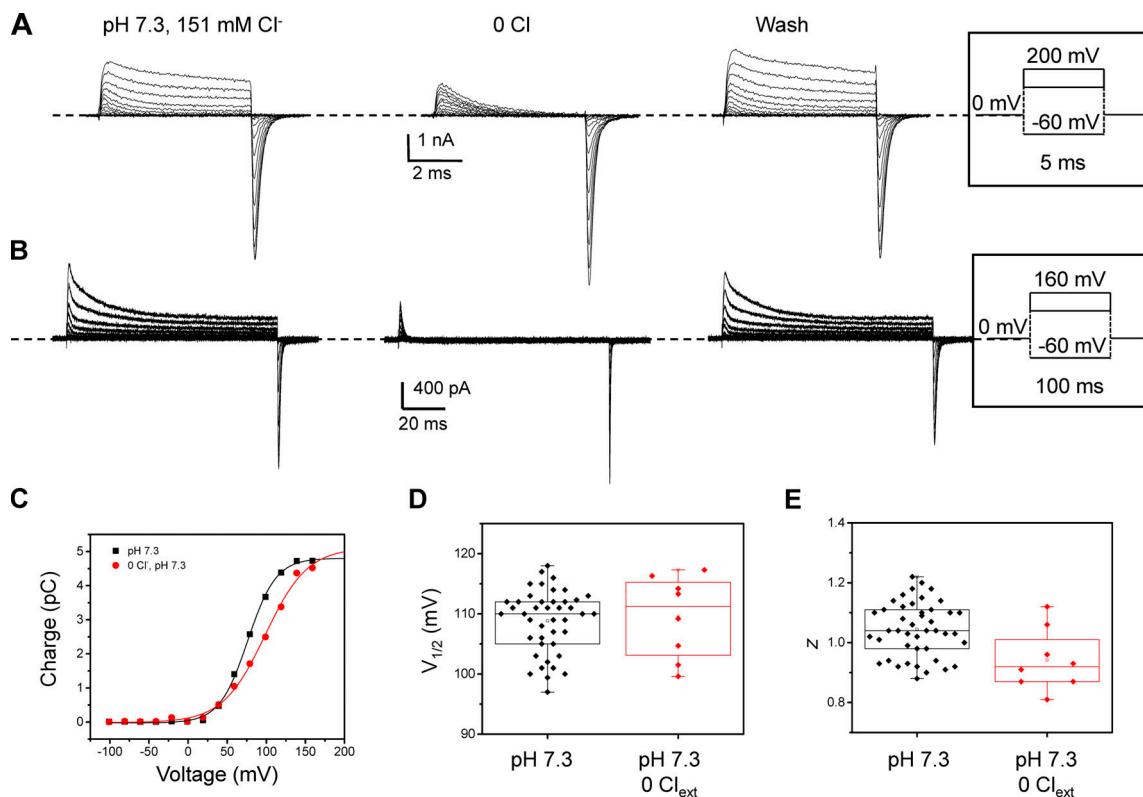


Figure 3. Cl^- dependence of transient and steady-state currents of mutant E312A. (A and B) Representative currents from the mutant E312A in control conditions and without extracellular Cl^- with test pulses of 5-ms duration (A) and 100-ms duration (B). Voltage protocols in A and B are shown as insets. (C) Charge measured upon return to the holding voltage (off charge) for the measurements shown in B with a test pulse duration of 5 ms. Lines represent fit with a Boltzmann function (see Materials and methods). (D) Box plots overlaid on original data show mean values of the voltage of half-maximal activation ($V_{1/2}$) for E312A in control conditions and without extracellular Cl^- . (E) Box plots overlaid on original data show mean values of the apparent gating charge (z).

Steady-state currents in E312A

As mentioned above, different from the behavior of ClC-3, ClC-4, ClC-5, and ClC-6, for the proton glutamate mutant E312A of ClC-7 we detected also steady-state transport currents. We initially characterized these currents using voltage steps of either 5-ms or 1-s duration as these were the voltage protocols that in the WT allowed for the characterization of transient currents and steady-state currents; however, for E312A the current kinetics could be adequately followed by steps of 100-ms duration (Figs. 3 B and 4 A). This voltage protocol revealed complex current kinetics with a peak reached almost instantaneously followed by a decay to a steady-state level within ~ 50 ms (Fig. 3 B). At 160 mV, the ratio between peak and steady-state current for steps of 100-ms duration is 3.1 ± 0.3 ($n = 30$, SEM).

Several lines of evidence indicate that the currents observed are specific to the E312A construct and not due to leak or unspecific conductances. First, currents similar to that of E312A were not elicited in 42 mock-transfected cells subject to the same voltage protocol or exposed to extracellular solutions of different pH or without Cl^- (Fig. S3 and Fig. S4). Second, the magnitude of steady-state currents—measured at 160 mV after 100 ms from the beginning of the voltage step—strongly correlates with the maximum charge of the transient currents (Fig. S2 B). Third, stationary E312A currents are clearly outwardly rectifying, like ClC-7, although with a blunted voltage dependence (Fig. 3, A and

B; and Fig. S4). This is directly illustrated in the I-V relationship obtained from raw currents of E312A and mock-transfected cells (without application of the P/N leak subtraction; Fig. S4). In addition, the figure shows that the small currents observed for E312A in the negative voltage range are indistinguishable from those in mock-transfected cells. Fourth, as expected for a Cl^-/H^+ antiporter, the E312A steady-state currents are almost abolished in the absence of extracellular Cl^- (Fig. 3, A and B; and Fig. S4). Regarding the effect of extracellular pH, we consistently found that pH 8.3 and pH 6.3 do not affect the steady-state current but have a strong effect on current kinetics (Fig. 4 A). Compared with pH 7.3, at pH 8.3 the peak current decreases and at pH 6.3 is abolished.

Transient currents do not depend on the length of the activating pulse

The voltage steps used to study the transient currents in the WT have a duration of only 5 ms, whereas ClC-7 transport currents activate with a time constant on the order of several seconds. Mechanistically, an important question is whether the transient currents depend on the gating status of the transporter—that is, if there is a relationship between the activation of transport activity and the magnitude of transient capacitive currents. To investigate this, we measured transient inward currents at 0 mV after applying voltage pulses to 140 mV of increasing duration

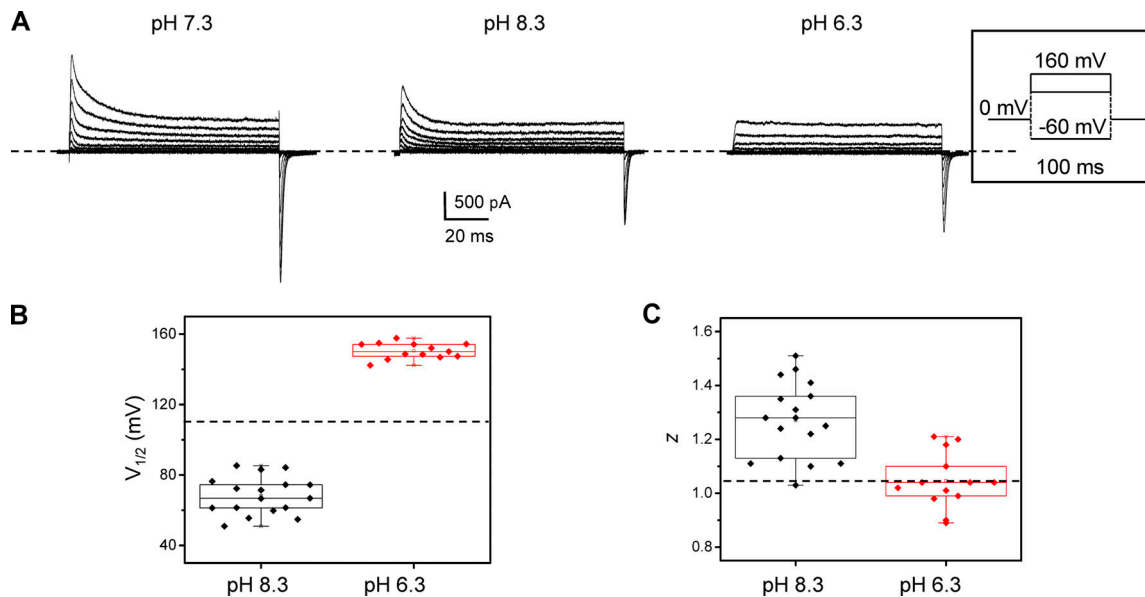


Figure 4. **pH dependence of transient and steady-state currents of mutant E312A.** (A) Representative current traces of the mutant E312A in control conditions and at pH 8.3 and pH 6.3. Currents were elicited with test pulses of 100-ms duration (the voltage protocol is shown as inset). (B) Mean values of the voltage of half-maximal activation ($V_{1/2}$) at pH 8.3 and pH 6.3 extracted as explained in Fig. 2. For comparison, the mean value at pH 7.3 shown in Fig. 3 D is included here as a dashed line. (C) Mean values of the voltage of the apparent gating charge (z) at pH 8.3 and pH 6.3 obtained as in Fig. 2. For comparison, the mean value at pH 7.3 shown in Fig. 3 E is included here as a dashed line.

from 0.1 to 330 ms. Fig. 5 A shows three representative current traces for pulses to 140 mV of 30-, 220-, and 330-ms duration, respectively, with the inset illustrating on a magnified timescale the transient capacitive currents elicited by stepping back the voltage to the holding potential. These measurements clearly show the slow activation of transport activity that is typical of CLC-7 and that, despite a very different degree of activation, the transient capacitive currents are qualitatively very similar. This conclusion is supported by the quantitative analysis shown in Fig. 5 B in which the charge associated with the transient capacitive current was extracted from similar recordings with pulse durations ranging from 0.1 to 330 ms and then normalized and averaged. It can be observed that the charge increases for the first 10 pulses (pulse duration from 0.1 ms to 5.8 ms) and this initial increase is characterized by a time constant on the order of 1 ms when fitted with a single exponential function (data not shown). After ~5 ms, the charge reached saturation and did not significantly change with longer activation pulses, whereas the current associated with transport did not reach steady state even after 330 ms. To explore this phenomenon in more detail, we took advantage of the phenotype of the osteopetrosis-associated mutation R760Q, which is characterized by much faster activation kinetics of transport currents (Leisle et al., 2011). Fig. 5 C shows that the R760Q mutant displays similar transient capacitive currents compared with WT. Importantly, and also similar to WT, these transient currents are similar for the three time points shown in the figure, although, different from WT, the steady-state current is almost in saturation already after 50 ms. Fig. 5 D shows the same statistical analysis performed for the WT and illustrates that the charge associated with the

transient currents is independent of the degree of activation of steady-state current also for R760Q.

Discussion

The three main conclusions of this work are (1) that WT (plasma membrane directed) CLC-7 exhibits transient capacitive currents when expressed in HEK293 cells; (2) in CLC-7, the substitution with alanine of the proton glutamate (E312A) does not abolish transport activity (CLC-7 is the only CLC transporter for which this behavior has emerged so far); and (3) the E312A mutant exhibits transient currents that are very similar to those of the WT.

Transient capacitive currents have also been measured for CLC-3, CLC-4, and CLC-5 with $V_{1/2}$ values of 75, 78, and 129 mV, respectively, in control conditions (Guzman et al., 2013). This is on the same order of magnitude as we find here for CLC-7 (110 mV).

To study in more detail the transient capacitive currents, we mutated the conserved proton glutamate of CLC-7 into alanine (E312A). The corresponding mutation inhibits proton transport in the bacterial CLC-ec1 transporter and abolishes transport altogether in the mammalian antiporters CLC-3, CLC-4, CLC-5, and CLC-6 (Lim and Miller, 2009; Accardi et al., 2005; Zdebik et al., 2008; Neagoe et al., 2010; Guzman et al., 2013). In particular, in CLC-5, this mutation (E268A) was used as a tool to isolate and study in detail transient capacitive currents, which are almost undetectable in the WT (Smith and Lippiat, 2010; Zifarelli et al., 2012). Interestingly, E312A transient currents are quantitatively very similar to those observed in WT CLC-7, as changing pH_{ext} leads to similar shifts of the $Q(V)$ curve, whereas removal of

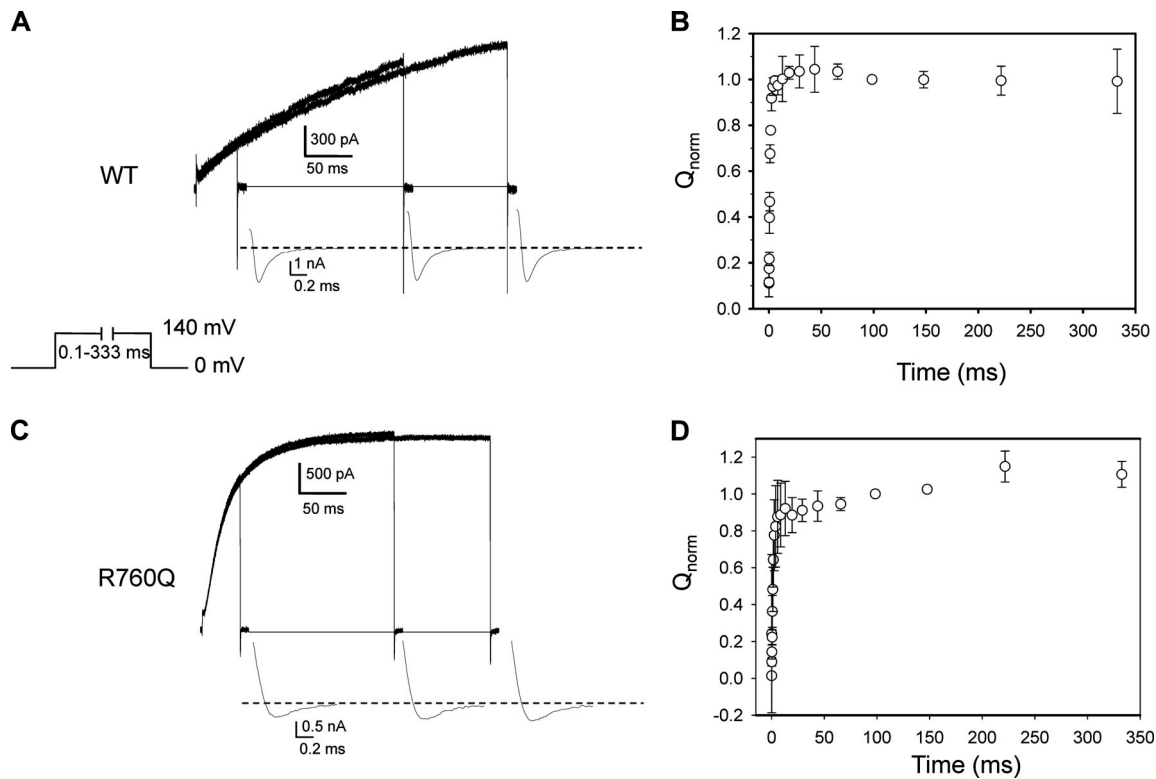


Figure 5. Dependence of transient capacitive currents on the duration of the activating pulse for WT and the R760Q mutation. (A) Three representative recordings with duration of the activating pulse of 30, 220, and 330 ms. Transient capacitive currents are shown as insets on a magnified timescale. The voltage protocol is shown as inset. **(B)** Mean values of the normalized charge (Q_{norm}) associated with the transient capacitive currents of WT CLC-7 calculated as in Fig. 2. Normalization was performed with the data point at 100 ms ($n = 4$). **(C)** Representative recordings of steady-state current from the mutant R760Q with duration of the activating pulse of 30, 220, and 330 ms. Transient capacitive currents are shown as insets on a magnified timescale. **(D)** Mean values of the charge associated with the transient capacitive currents of the R760Q mutant calculated as for the WT ($n = 3$).

Cl^-_{ext} does not have any substantial effect. This contrasts with the behavior of the proton glutamate mutant (E268A) of CLC-5, in which $V_{1/2}$ was less affected by pH_{ext} but shifted by ~ 50 mV to more positive voltages upon removing Cl^-_{ext} , with transient currents becoming progressively smaller in amplitude at low Cl^-_{ext} (Zifarelli et al., 2012). In this respect, it is intriguing that the apparent gating charge z associated with the transient currents of CLC-7 is ~ 1 (practically independent of extracellular ionic conditions), which is considerably reduced compared with the value that $z \sim 1.5$ observed for the E268A mutant of CLC-5. Thus, while the dependence on $[\text{Cl}^-]_{\text{int}}$ seems to be a common property of CLC transporter capacitive currents, the lack of $[\text{Cl}^-]_{\text{ext}}$ dependence in CLC-7 indicates that the details of the process underlying the transient currents in CLC-7 are different from those of the E268A mutant of CLC-5. The transient capacitive currents of CLC-5 E268A have been explained in terms of a model in which the movement of an intrinsic gating charge, most likely the gating glutamate E211, associated with an inward movement of a bound Cl^- ion, is followed by a voltage-dependent, low-affinity binding of extracellular Cl^- ions (Zifarelli et al., 2012). To investigate possible differences between the mechanisms generating transient currents in CLC-5 and CLC-7, we mutated the gating glutamate of CLC-7 to alanine (E245A). As already illustrated by Leisle et al. (2011) and consistent with the finding in all CLC transporters (Accardi et al., 2004; Piccolo and Pusch,

2005; Scheel et al., 2005; Neagoe et al., 2010; Leisle et al., 2011), this mutation turned CLC-7 into a purely ohmic conductance and did not show any transient capacitive current (Fig. S5). This supports the critical role of the gating glutamate in generating the transient capacitive currents of CLC-7 and is consistent with the model proposed for CLC-5. Moreover, it indicates that the quantitative difference in the effect of Cl^-_{ext} on CLC-7 and CLC-5 might be the result of subtle structural differences between the two transporters. CLC-7 is the only mammalian CLC transporter associated with a β subunit, and two recent structures of CLC-7 in complex with Ostml indicate that Ostml has some functional effects on CLC-7 (Schrecker et al., 2020; Zhang et al., 2020). In particular, Schrecker et al. (2020) found some structural rearrangements in the permeation pathway with altered Cl^- ion occupancy of the external and central binding sites. While it can be speculated that these effects of Ostml are sufficient to explain the different effect of Cl^-_{ext} on the capacitive currents of CLC-5 and CLC-7, more detailed studies are necessary to fully elucidate this point. Furthermore, in the structure of CLC-7/Ostml reported by Schrecker et al. (2020), the side chain of the gating glutamate occupies an external position displaced from the permeation pathway, a conformation that has so far only been found for a structure of CLC-ecl in which the gating glutamate was mutated to glutamine (Dutzler et al., 2003). While the structure of CLC-5 is unknown, it is likely

more closely related to CLC-ec1 than CLC-7, and it can be speculated that different resting conformations of the gating glutamate are partially responsible for quantitative differences of the respective transient currents.

Among mammalian CLC transporters, CLC-7 is unique as being characterized by a very slow activation of transport currents at positive voltages (Leisle et al., 2011). The slow activation is indicative of a gating process that is able to switch the transporter between an actively transporting state and an inactive state. The nature of this gate appears to be similar to the common gating mechanism of CLC channels in that it depends on both subunits of the dimeric transporter (Miller, 1982; Saviane et al., 1999; Ludwig et al., 2013). Such a gating process, even though much faster, has been proposed to also be present in CLC-5 (De Stefano et al., 2013). Importantly, the slow kinetics of CLC-7 gating allow for an investigation of a possible correlation of gate activation and transient capacitive currents. Somewhat surprisingly, we found that for vastly different levels of activation of transport current, the charge movement associated with the transient capacitive currents remains remarkably similar and only changes during the first 5 ms, which indicates that the transient capacitive currents of CLC-7 are independent of the degree of transport activity (Fig. 5, A and B). This conclusion is further supported by measurements of the mutant R760Q that exhibits much faster transport activation kinetics compared with WT (Fig. 5, C and D). The independence of transport activity and transient capacitive currents in CLC-7 is difficult to reconcile with the model proposed for CLC-5 in which the transient capacitive currents have been suggested to reflect a partial reaction of the transport cycle. The independence may suggest that the mechanism from which the transient currents originate is unrelated to transport; however, one key observation suggests that transient currents indeed reflect a partial reaction cycle: the fact that even when transport is not yet fully activated the transient currents do depend on $[Cl^-]_{int}$ and pH_{ext} (and those of CLC-5 on $[Cl^-]_{ext}$) indicates that an inactive transporter is still able to exchange Cl^- and H^+ substrate with the extracellular/luminal milieu and Cl^- ions with the cytosolic solution. Thus, to interrupt ion exchange in this inactive state, a speculative mechanism to reconcile several properties of common gating of CLC channels, gating of CLC transporters, and the properties of transient transporter currents, is that it is the closed state of the common gate which specifically impedes the exchange of cytosolic protons with the transporter/channel. Yet, clearly more information is needed to provide an explanation for these seemingly contrasting results. Unfortunately, a detailed kinetic analysis of the time dependence of the transient capacitive currents is precluded by the limited time resolution of whole-cell patch-clamp measurements; however, a few considerations regarding transport kinetics are warranted. First, the kinetics of transient currents are on the millisecond or sub-millisecond timescale. Thus, if these are related to the transport cycle, turnover of an active transporter can be estimated to be on the order or greater than $\sim 10^3 s^{-1}$. An independent estimate of the turnover can be obtained from the slope of the correlation of transport current versus maximal transient charge (compare with Fig. S2), yielding a value of $640 s^{-1}$. Given a 2 Cl^- :1 H^+

stoichiometry, the transient charge of a single transporter is expected to be three or fewer elementary charges, reducing the estimate of the turnover rate to $640 s^{-1} / 3 = 213 s^{-1}$. However, for the latter figure it has to be kept in mind that the current was measured 500 ms after stepping the voltage to 100 mV, a time at which the transporter has not yet achieved steady state and at which the maximal activation probability is well below unity. Thus, this approach yields a somewhat speculative estimate of turnover of an active transporter again on the order of $10^3 s^{-1}$, which is consistent with the estimate provided by the kinetics of the transient currents. This value is of similar magnitude as that found for the bacterial CLC-ec1 (Walden et al., 2007) but much smaller compared with what has been inferred from nonstationary noise analysis of CLC-5 ($10^5 s^{-1}$; Zdebik et al., 2008).

Another surprising finding of this study is that, unlike all the other mammalian CLC transporters characterized so far, we could detect ionic currents for the proton glutamate mutation (E312A) of CLC-7. These currents have completely different kinetics compared with WT, with a very fast activation followed by a partial inactivation that results in steady-state currents. The steady-state currents are much smaller than those for WT, but, as detailed in Results, several lines of evidence strongly suggest that the currents observed are specific to the E312A construct and not a result of leak or other conductances. Regarding the current rectification, a detailed comparison of currents from E312A and mock-transfected cells without leak subtraction (Fig. S4) shows that the currents elicited in the negative voltage range are superimposable and were not modified by removal of Cl^- from the extracellular solution (Fig. S4 C). We therefore conclude that, consistent with previous results for WT CLC-7 (Leisle et al., 2011), E312A is strongly outwardly rectifying. CLC-7 is the first mammalian CLC transporter in which mutation of the proton glutamate to alanine does not abolish stationary Cl^- transport. This finding potentially explains why the E312A KI mouse line, while still affected by osteopetrosis like CLC-7 KO, has a milder phenotype and normal fur pigmentation (Weinert et al., 2014). The issue is highly relevant because, under the assumption that the E312A mutation will abolish transport activity, the different phenotypes of CLC-7 KO and E312A KI have previously led to the suggestion that the physiological role of CLC-7 is not only to provide lysosomal ion transport but also to serve as a scaffolding unit in macromolecular complexes in the lysosomal membrane (Weinert et al., 2014). In contrast to this, our results suggest that the residual activity of E312A might be sufficient to rescue some of the physiological functions compromised in CLC-7 KO mice.

Acknowledgments

Merritt Maduke served as editor.

We thank Damiano Migliozi and Francesca Quartino for technical assistance, Raffaella Barbieri and Sara Bertelli for assisting with cell culture, and Maddalena Comini for critical reading of the manuscript.

This work was supported by Physiological Society (UK) grant 444, Medical Research Fund (UK) grant 23/2016 (to G. Zifarelli), Fondazione AIRC per la Ricerca sul Cancro grant IG 21558, and

Italian Research Ministry grant PRIN 20174TB8KW (to M. Pusch).

The authors declare no competing financial interests.

Author contributions: M. Pusch and G. Zifarelli designed and performed experiments, analyzed data, and wrote the manuscript.

Submitted: 5 February 2020

Revised: 28 September 2020

Accepted: 28 October 2020

References

- Accardi, A., and M. Pusch. 2003. Conformational changes in the pore of CLC-0. *J. Gen. Physiol.* 122:277–294. <https://doi.org/10.1085/jgp.200308834>
- Accardi, A., L. Kolmakova-Partensky, C. Williams, and C. Miller. 2004. Ionic currents mediated by a prokaryotic homologue of CLC Cl⁻ channels. *J. Gen. Physiol.* 123:109–119. <https://doi.org/10.1085/jgp.200308935>
- Accardi, A., M. Walden, W. Nguitragool, H. Jayaram, C. Williams, and C. Miller. 2005. Separate ion pathways in a Cl⁻/H⁺ exchanger. *J. Gen. Physiol.* 126:563–570. <https://doi.org/10.1085/jgp.200509417>
- Bezanilla, F. 2008. How membrane proteins sense voltage. *Nat. Rev. Mol. Cell Biol.* 9:323–332. <https://doi.org/10.1038/nrm2376>
- De Stefano, S., M. Pusch, and G. Zifarelli. 2013. A single point mutation reveals gating of the human CLC-5 Cl⁻/H⁺ antiporter. *J. Physiol.* 591: 5879–5893. <https://doi.org/10.1113/jphysiol.2013.260240>
- Dutzler, R., E.B. Campbell, M. Cadene, B.T. Chait, and R. MacKinnon. 2002. X-ray structure of a CLC chloride channel at 3.0 Å reveals the molecular basis of anion selectivity. *Nature*. 415:287–294. <https://doi.org/10.1038/415287a>
- Dutzler, R., E.B. Campbell, and R. MacKinnon. 2003. Gating the selectivity filter in CLC chloride channels. *Science*. 300:108–112. <https://doi.org/10.1126/science.1082708>
- Feng, L., E.B. Campbell, Y. Hsiung, and R. MacKinnon. 2010. Structure of a eukaryotic CLC transporter defines an intermediate state in the transport cycle. *Science*. 330:635–641. <https://doi.org/10.1126/science.1195230>
- Graves, A.R., P.K. Curran, C.L. Smith, and J.A. Mindell. 2008. The Cl⁻/H⁺ antiporter CLC-7 is the primary chloride permeation pathway in lysosomes. *Nature*. 453:788–792. <https://doi.org/10.1038/nature06907>
- Grieschat, M., and A.K. Alekov. 2012. Glutamate 268 regulates transport probability of the anion/proton exchanger CLC-5. *J. Biol. Chem.* 287: 8101–8109. <https://doi.org/10.1074/jbc.M111.298265>
- Günther, W., A. Lüchow, F. Cluzeaud, A. Vandewalle, and T.J. Jentsch. 1998. CLC-5, the chloride channel mutated in Dent's disease, colocalizes with the proton pump in endocytically active kidney cells. *Proc. Natl. Acad. Sci. USA*. 95:8075–8080. <https://doi.org/10.1073/pnas.95.14.8075>
- Guzman, R.E., M. Grieschat, C. Fahlke, and A.K. Alekov. 2013. CLC-3 is an intracellular chloride/proton exchanger with large voltage-dependent nonlinear capacitance. *ACS Chem. Neurosci.* 4:994–1003. <https://doi.org/10.1021/cn400032z>
- Hryciw, D.H., Y. Wang, O. Devuyst, C.A. Pollock, P. Poronnik, and W.B. Guggino. 2003. Cofilin interacts with CLC-5 and regulates albumin uptake in proximal tubule cell lines. *J. Biol. Chem.* 278:40169–40176. <https://doi.org/10.1074/jbc.M307890200>
- Jentsch, T.J., and M. Pusch. 2018. CLC Chloride Channels and Transporters: Structure, Function, Physiology, and Disease. *Physiol. Rev.* 98:1493–1590. <https://doi.org/10.1152/physrev.00047.2017>
- Kasper, D., R. Planells-Cases, J.C. Fuhrmann, O. Scheel, O. Zeitz, K. Ruether, A. Schmitt, M. Poët, R. Steinfeld, M. Schweizer, et al. 2005. Loss of the chloride channel CLC-7 leads to lysosomal storage disease and neurodegeneration. *EMBO J.* 24:1079–1091. <https://doi.org/10.1038/sj.emboj.7600576>
- Kornak, U., D. Kasper, M.R. Bösl, E. Kaiser, M. Schweizer, A. Schulz, W. Friedrich, G. Dellling, and T.J. Jentsch. 2001. Loss of the CLC-7 chloride channel leads to osteopetrosis in mice and man. *Cell*. 104:205–215. [https://doi.org/10.1016/S0092-8674\(01\)00206-9](https://doi.org/10.1016/S0092-8674(01)00206-9)
- Lange, P.F., L. Wartosch, T.J. Jentsch, and J.C. Fuhrmann. 2006. CLC-7 requires Ostml as a beta-subunit to support bone resorption and lysosomal function. *Nature*. 440:220–223. <https://doi.org/10.1038/nature04535>
- Leisle, L., C.F. Ludwig, F.A. Wagner, T.J. Jentsch, and T. Stauber. 2011. CLC-7 is a slowly voltage-gated 2Cl⁻/1H⁺-exchanger and requires Ostml for transport activity. *EMBO J.* 30:2140–2152. <https://doi.org/10.1038/emboj.2011.137>
- Lim, H.H., and C. Miller. 2009. Intracellular proton-transfer mutants in a CLC Cl⁻/H⁺ exchanger. *J. Gen. Physiol.* 133:131–138. <https://doi.org/10.1085/jgp.200810112>
- Ludwig, C.F., F. Ullrich, L. Leisle, T. Stauber, and T.J. Jentsch. 2013. Common gating of both CLC transporter subunits underlies voltage-dependent activation of the 2Cl⁻/1H⁺ exchanger CLC-7/Ostml. *J. Biol. Chem.* 288: 28611–28619. <https://doi.org/10.1074/jbc.M113.509364>
- Miller, C. 1982. Open-state substructure of single chloride channels from Torpedo electroplax. *Philos. Trans. R. Soc. Lond. B Biol. Sci.* 299:401–411. <https://doi.org/10.1098/rstb.1982.0140>
- Neage, I., T. Stauber, P. Fidzinski, E.Y. Bergsdorf, and T.J. Jentsch. 2010. The late endosomal CLC-6 mediates proton/chloride countertransport in heterologous plasma membrane expression. *J. Biol. Chem.* 285: 21689–21697. <https://doi.org/10.1074/jbc.M110.125971>
- Park, E., and R. MacKinnon. 2018. Structure of the CLC-1 chloride channel from *Homo sapiens* eLife. 7:e36629. <https://doi.org/10.7554/eLife.36629>
- Park, E., E.B. Campbell, and R. MacKinnon. 2017. Structure of a CLC chloride ion channel by cryo-electron microscopy. *Nature*. 541:500–505. <https://doi.org/10.1038/nature20812>
- Piccolo, A., and M. Pusch. 2005. Chloride/proton antiporter activity of mammalian CLC proteins CLC-4 and CLC-5. *Nature*. 436:420–423. <https://doi.org/10.1038/nature03720>
- Saviane, C., F. Conti, and M. Pusch. 1999. The muscle chloride channel CLC-1 has a double-barreled appearance that is differentially affected in dominant and recessive myotonia. *J. Gen. Physiol.* 113:457–468. <https://doi.org/10.1085/jgp.113.3.457>
- Scheel, O., A.A. Zdebik, S. Lourdel, and T.J. Jentsch. 2005. Voltage-dependent electrogenic chloride/proton exchange by endosomal CLC proteins. *Nature*. 436:424–427. <https://doi.org/10.1038/nature03860>
- Schrecker, M., J. Korobenko, and R.K. Hite. 2020. Cryo-EM structure of the lysosomal chloride-proton exchanger CLC-7 in complex with OSTML. *eLife*. 9:e59555. <https://doi.org/10.7554/eLife.59555>
- Smith, A.J., and J.D. Lippiat. 2010. Voltage-dependent charge movement associated with activation of the CLC-5 2Cl⁻/1H⁺ exchanger. *FASEB J.* 24: 3696–3705. <https://doi.org/10.1096/fj.09-150649>
- Stauber, T., and T.J. Jentsch. 2010. Sorting motifs of the endosomal/lysosomal CLC chloride transporters. *J. Biol. Chem.* 285:34537–34548. <https://doi.org/10.1074/jbc.M110.162545>
- Walden, M., A. Accardi, F. Wu, C. Xu, C. Williams, and C. Miller. 2007. Uncoupling and turnover in a Cl⁻/H⁺ exchange transporter. *J. Gen. Physiol.* 129:317–329. <https://doi.org/10.1085/jgp.200709756>
- Wang, K., S.S. Preisler, L. Zhang, Y. Cui, J.W. Missel, C. Grønberg, K. Gotfryd, E. Lindahl, M. Andersson, K. Calloe, et al. 2019. Structure of the human CLC-1 chloride channel. *PLoS Biol.* 17:e3000218. <https://doi.org/10.1371/journal.pbio.3000218>
- Weinert, S., S. Jabs, C. Supanchart, M. Schweizer, N. Gimber, M. Richter, J. Rademann, T. Stauber, U. Kornak, and T.J. Jentsch. 2010. Lysosomal pathology and osteopetrosis upon loss of H⁺-driven lysosomal Cl⁻ accumulation. *Science*. 328:1401–1403. <https://doi.org/10.1126/science.1188072>
- Weinert, S., S. Jabs, S. Hohensee, W.L. Chan, U. Kornak, and T.J. Jentsch. 2014. Transport activity and presence of CLC-7/Ostml complex account for different cellular functions. *EMBO Rep.* 15:784–791. <https://doi.org/10.15252/embr.201438553>
- Zanardi, I., G. Zifarelli, and M. Pusch. 2013. An optical assay of the transport activity of CLC-7. *Sci. Rep.* 3:1231. <https://doi.org/10.1038/srep01231>
- Zdebik, A.A., G. Zifarelli, E.Y. Bergsdorf, P. Soliani, O. Scheel, T.J. Jentsch, and M. Pusch. 2008. Determinants of anion-proton coupling in mammalian endosomal CLC proteins. *J. Biol. Chem.* 283:4219–4227. <https://doi.org/10.1074/jbc.M708368200>
- Zhang, S., Y. Liu, B. Zhang, J. Zhou, T. Li, Z. Liu, Y. Li, and M. Yang. 2020. Molecular insights into the human CLC-7/Ostml transporter. *Sci. Adv.* 6: eabb4747. <https://doi.org/10.1126/sciadv.abb4747>
- Zifarelli, G., and M. Pusch. 2007. CLC chloride channels and transporters: a biophysical and physiological perspective. *Rev. Physiol. Biochem. Pharmacol.* 158:23–76. https://doi.org/10.1007/112_2006_0605
- Zifarelli, G., S. De Stefano, I. Zanardi, and M. Pusch. 2012. On the mechanism of gating charge movement of CLC-5, a human Cl⁻/H⁺ antiporter. *Bioophys. J.* 102:2060–2069. <https://doi.org/10.1016/j.bpj.2012.03.067>

Supplemental material

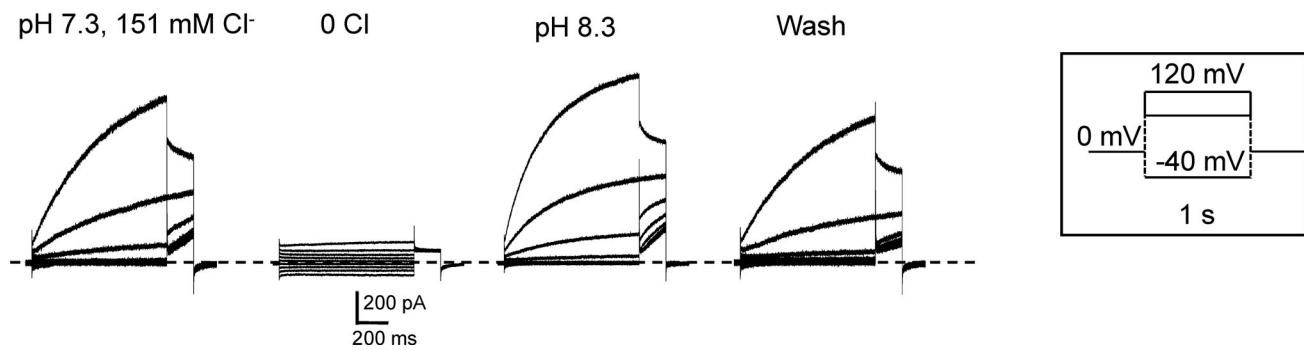


Figure S1. **Representative measurements of steady-state currents from CLC-7 in different extracellular solutions as indicated.** Currents were elicited with test pulses of 1-s duration (the voltage protocol is shown as inset).

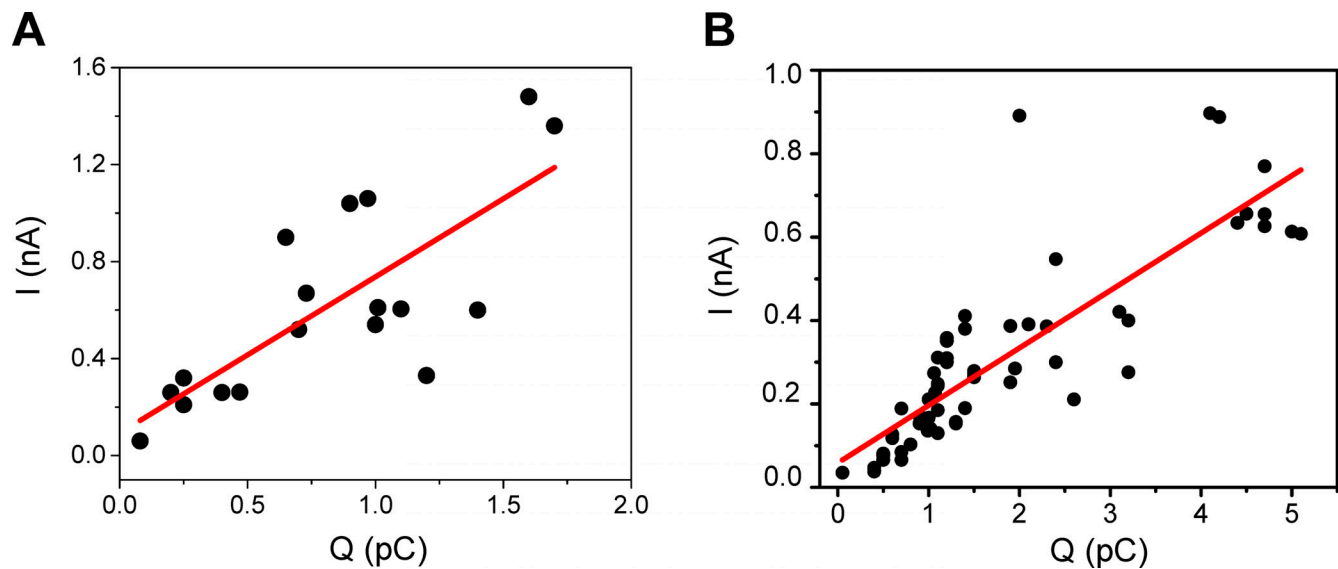


Figure S2. **Correlation between steady-state current and off charge of the transient inward currents.** (A) For the WT, the correlation is between steady-state current elicited by a voltage step to 100 mV measured after 500 ms and off charge after a 5-ms voltage step to 200 mV ($r^2 = 0.56$; slope, $640 \pm 140 \text{ s}^{-1}$). (B) For E312A, the correlation is between steady-state current measured at the end of the 100-ms r^2 test pulse to 160 mV and the off charge after the same voltage step ($r^2 = 0.77$; slope, $137 \pm 15 \text{ s}^{-1}$).

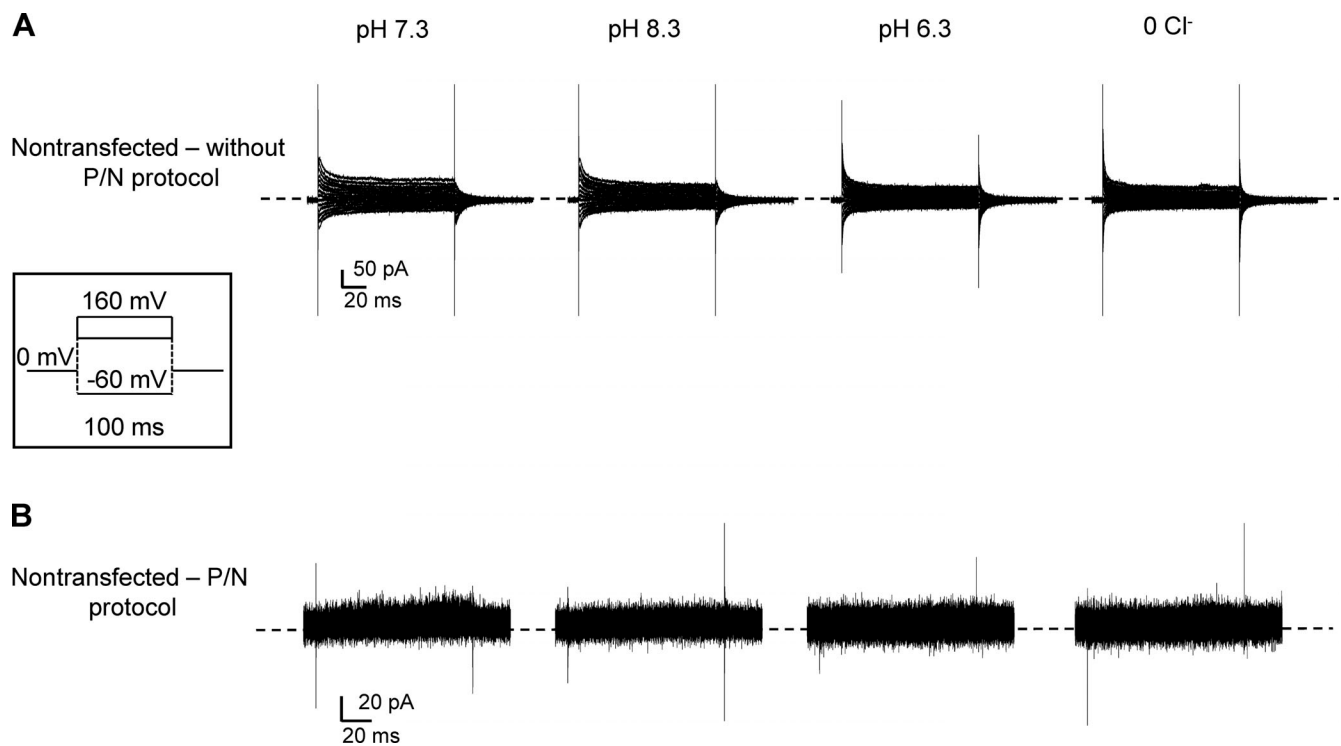


Figure S3. **Effect of the P/N protocol on currents from nontransfected cells in solutions of different ionic composition.** (A) Upper traces are representative recordings from the same cell in solutions at pH 7.3, 8.3, and 6.3 and without Cl⁻ with application of the standard voltage protocol (shown as inset) and without P/N subtraction. (B) Same recordings as in A, but with application of the P/N protocol.

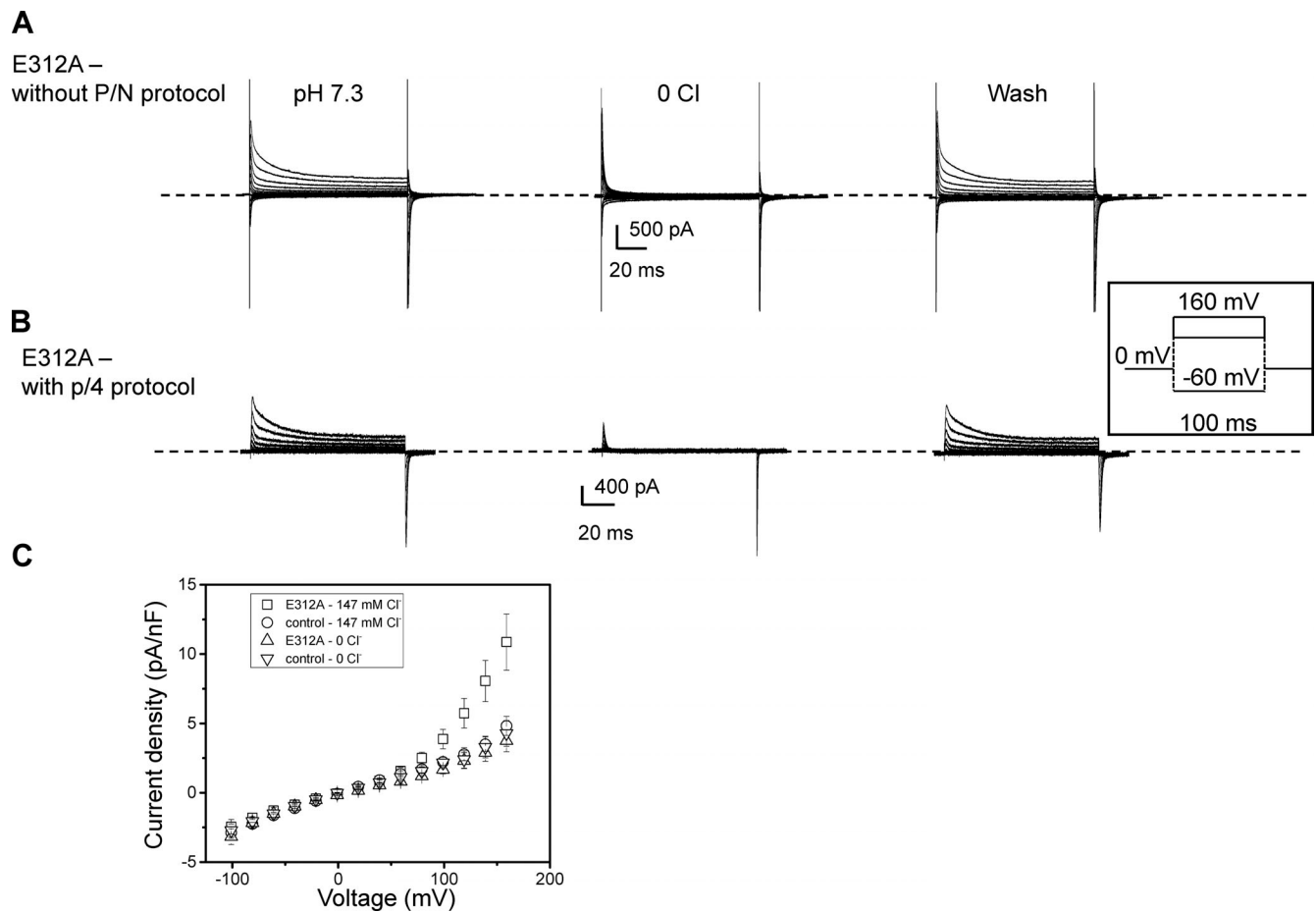


Figure S4. **Effect of the P/N protocol on currents from E312A.** **(A)** Representative recordings from E312A without P/N subtraction in standard solution, without Cl⁻, and back to standard solution. The voltage protocol is shown as inset. **(B)** Same recordings as in A, but with application of the P/N protocol. **(C)** Averaged current-voltage relationship for E312A ($n = 8$) and mock-transfected cells ($n = 12$) obtained from measurements without application of the P/N protocol.

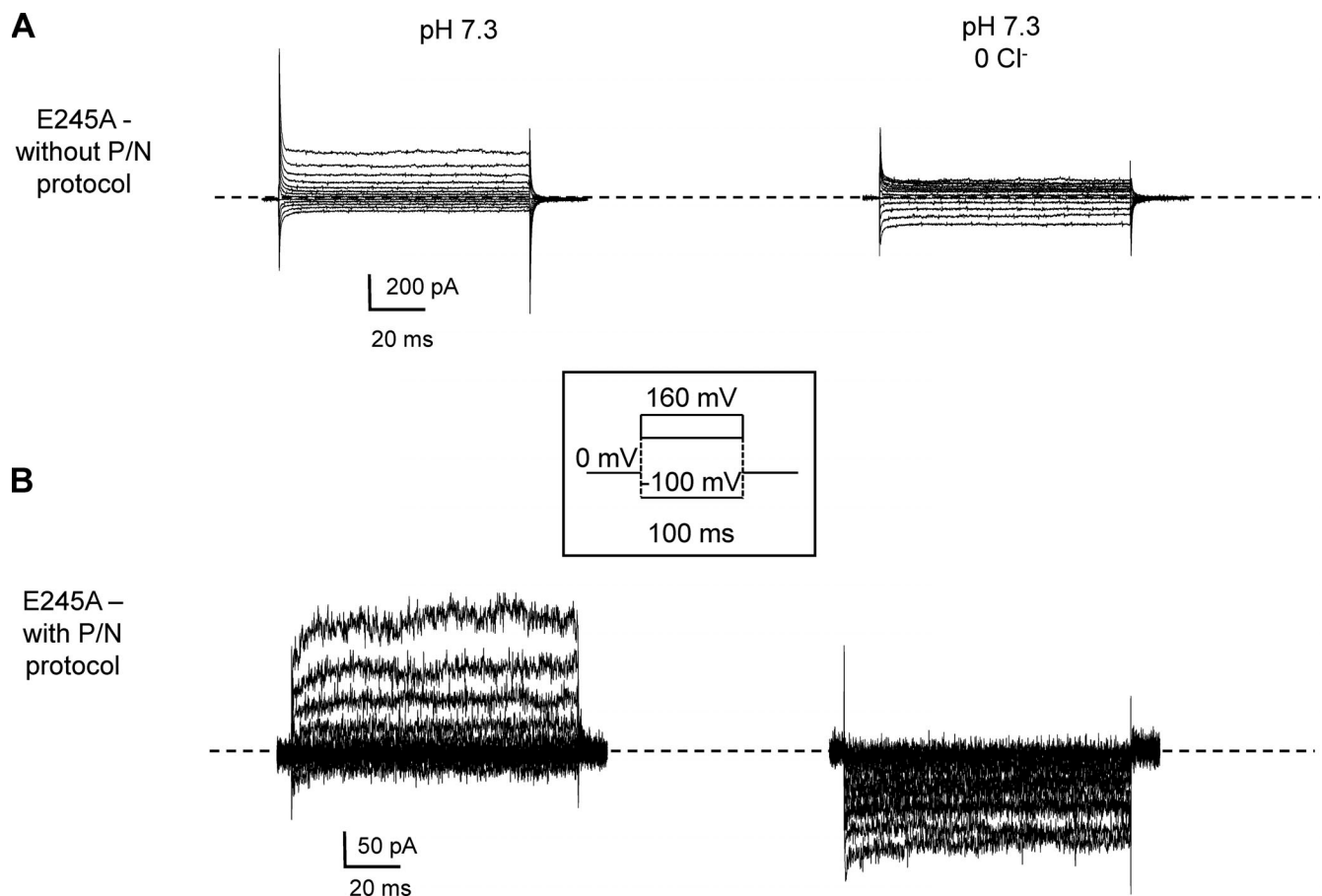


Figure S5. **Effect of the P/N protocol on currents from E245A. (A)** Representative recordings from E245A without P/N subtraction in standard solution and without Cl⁻. The voltage protocol is shown as inset. **(B)** Same recordings as in A, but with application of the P/N protocol.